Stem Cell Reports
Report

ISSCR

OPEN ACCESS

Astrocytes Attenuate Mitochondrial Dysfunctions in Human Dopaminergic Neurons Derived from iPSC

Fang Du,[1,2] Qing Yu,[1,2] Allen Chen,[1] Doris Chen,[1] and Shirley ShiDu Yan[1,*]
[1]Department of Pharmacology and Toxicology, and Higuchi Bioscience Center, School of Pharmacy, University of Kansas, 2099 Constant Avenue, Lawrence, KS 66047, USA
[2]Co-first author
*Correspondence: shidu@ku.edu
https://doi.org/10.1016/j.stemcr.2017.12.021

SUMMARY

Astrocytes, the most populous glial cell type in the brain, are critical for regulating the brain microenvironment. In various neurodegenerative diseases, astrocytes determine the progression and outcome of the neuropathological process. We have recently revealed the direct involvement of mitochondrial function in human pluripotent stem cell (hiPSC)-derived dopaminergic (DA) neuronal differentiation. Using the astroglial-neuronal co-culture system, we show here that astrocytes effectively rescue defects in neurogenesis of DA neurons with mitochondrial respiratory chain disruption. Co-culture of astrocytes with defective DA neurons completely restored mitochondrial functions and dynamics insulted by mitochondrial toxins. These results suggest the significance of astroglia in maintaining mitochondrial development and bioenergetics during differentiation of hiPSC-derived DA neurons. Our study also provides an active astroglial-neuronal interaction model for future investigation of mitochondrial involvement in neurogenesis and neurodegenerative diseases.

INTRODUCTION

Human pluripotent stem cells (hiPSCs) offer an attractive tool for modeling brain development and disease based on their ability to be directed and differentiated into human cerebral organoids and cells (Lancaster and Knoblich, 2014). Generated from hiPSCs, neural progenitor cells (NPCs) can be used to generate neuronal and glial cells (Maroof et al., 2013; Sofroniew and Vinters, 2010). Direction of these cells into specific cell types allows for identification of the underlying neuropathology and also presents the possibility of replacement therapy for neurodegenerative diseases such as Parkinson's disease (PD), which is caused by selective loss of dopaminergic (DA) neurons in the substantia nigra pars compacta in the midbrain (Kriks et al., 2011).

We have recently revealed (Fang et al., 2016a, 2016b) an active and pivotal role for mitochondria in midbrain DA and cortical neurogenesis. Induced defects in mitochondrial respiratory chains via application of a complex IV inhibitor, KCN (potassium cyanide), or complex I inhibitor, rotenone, restricted neurogenesis of DA neurons. Accumulating studies have demonstrated that astrocytes, the most populous glial cells and important coordinative partners to neighboring neuronal cells, are essential in DA neurogenesis in the subventricular zone of the lateral ventricles, a region for neurogenesis in the midbrain of adult brains, and disruption in astrocytic function promotes neurodegeneration (Lo, 2010). Here, we induced DA neuron differentiation with mature astrocyte co-culture, to mimic the *in vivo* neuronal-astroglial interaction environment. In the presence of astrocytes, NPCs were resistant to mitochondrial respiratory defects and exhibited normal differentiation into DA neurons. Importantly, using this dynamic astrocyte-neuron interaction model, we clearly display the essential role of mitochondria in DA neuronal differentiation and maturation. Furthermore, astrocytes actively modulate normal neuronal development by rescuing neuronal mitochondrial defects in the process of DA-directed differentiation. This human neuron-glia cross-talk model will facilitate evaluation of the role of astrocytes in modulating mitochondrial function in the pathogenesis of neurodegenerative diseases and identification of therapeutic applications in mitochondrial degeneration.

RESULTS

Efficient Differentiation of GFAP+ Mature Human Astrocytes from NPCs

We have previously shown that human DA neurons are derived from NPCs (Fang et al., 2016a). In this study, NPCs derived from BM2-3 hiPSCs were differentiated into astrocytes. Following the protocol shown in Figure S1A, S100β-positive cells were derived from astroglial progenitor cells after about 70 days induction with ciliary neurotrophic factor (CNTF) in astroglial medium (Figures S1B and S1C). Emergence of an astrocyte-like phenotype following 70 days induction was indicated by expression of the astrocyte markers S100β and GFAP (Figure S1A).

Populations of GFAP-positive astrocytes were robustly increased between the 3rd and the 9th month of differentiation by removing growth factors epidermal growth factor (EGF) and fibroblast growth factor 2 (FGF2) (Figures S1B and S1C). Definitive mature astrocytes with expression

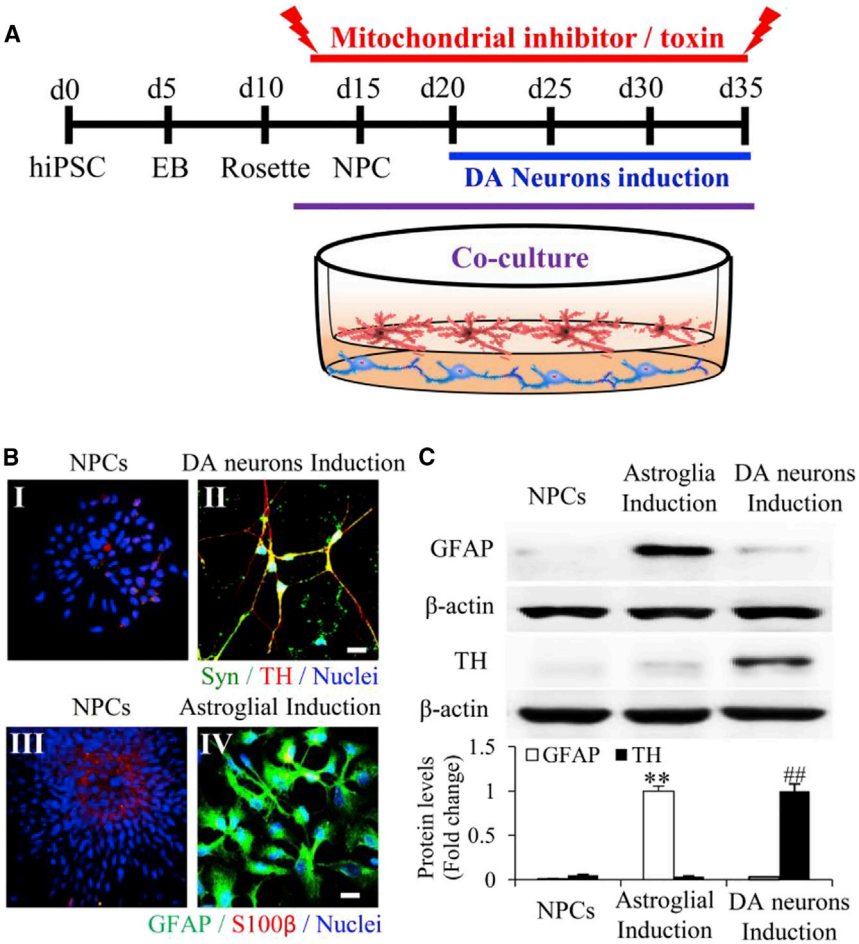

Figure 1. Differentiation and Development of hiPSC Line-Induced Human Dopaminergic Neurons and Astrocytes

(A) A schematic representation of the differentiation of mitochondrial inhibitor/toxin (KCN or rotenone)-treated hiPSC line-induced DA neurons with astroglial co-culture. EB, embryoid body.

(B) Immunocytochemistry of synaptophysin (Syn)-positive (green) puncta and TH (red) in neural progenitor cells (NPCs; **I**) and mature DA neurons (**II**) and mature astroglial marker (GFAP, green) and astroglial progenitor marker (S100β, red) in NPCs (**III**) and astrocytes induced for 9 months (**IV**).

(C) Representative immunoblots for GFAP and TH expression in NPCs, astrocytes induced for 9 months, and DA neurons. β-actin was used as a protein loading control. $^{**}p < 0.01$ versus NPCs and DA neurons (open bars, GFAP), and $^{\#\#}p < 0.01$ versus NPCs and DA neurons (black bars, TH).

Scale bars, 25 μm in (B). For (C), statistical analysis was performed using StatView software (SAS Institute, v.5.0.1). One-way ANOVA was used for repeated-measure analysis, followed by Fisher's protected least significant difference for post hoc comparisons. Data are presented as means ± SEM. n = 3 independent experiments.

of GFAP appeared 3 to 9 months following removal of growth factors EGF and FGF2 from astroglial medium (Figures S1B and S1C). Astrocyte maturation was characterized by the presence of the astrocyte marker GFAP (Figures 1B, 1C, and S1C). Quantification of GFAP-positive cells showed that the percentage of GFAP-expressing cells was 27.7% and 83.8% with 3 and 9 months of differentiation, respectively (quantification data not shown). In contrast, GFAP expression in human DA neuronal cultures was barely detected compared with astroglial culture (Figures 1C and S1D). DA neurons were verified by the absence of TH (tyrosine hydroxylase) expression in 9-month astroglial culture (Figures 1B, 1C, and S1D). Therefore, 9-month mature astrocytes were used in our co-culture system.

Co-culture with Astrocytes Rescues Impaired DA Neuronal Differentiation and Synaptogenesis

Accumulating evidence indicates the emerging role of astrocytes in the pathogenesis of neurological disorders, such as PD (Maragakis and Rothstein, 2006). Given the importance of mitochondrial respiratory function in DA neuron differentiation and synaptogenesis (Fang et al., 2016a), we investigated the effect of astrocytes on DA neuronal development under respiratory chain impairment using a neuron-astrocyte co-culture system. Impairment of mitochondrial respiratory function was induced by the addition of inhibitor for complex IV (KCN, 500 nM) and complex I (rotenone, 10 nM), as we previously described (Fang et al., 2016a). Consistent with our previous results, KCN- or rotenone-induced inhibition of mitochondrial respiratory function significantly suppressed synapse development and maturation of DA neurons. However, with astrocyte co-culture, the lengths of MAP2 (a marker for neuronal dendrites)- and TH (a marker for DA neurons)-positive processes of neurons were significantly longer compared with those neurons without astrocyte co-culture in the presence of KCN or rotenone (Figures 2A and 2B). The number of synaptophysin-positive puncta in TH dendrites was also significantly increased (Figures 2A and 2C). Accordingly, quantitative real-time PCR showed that levels of mature DA neuronal markers, including *aromatic L-amino acid decarboxylase* (*AADC*), *dopamine transporter* (*DAT*), and *vesicular monoamine*

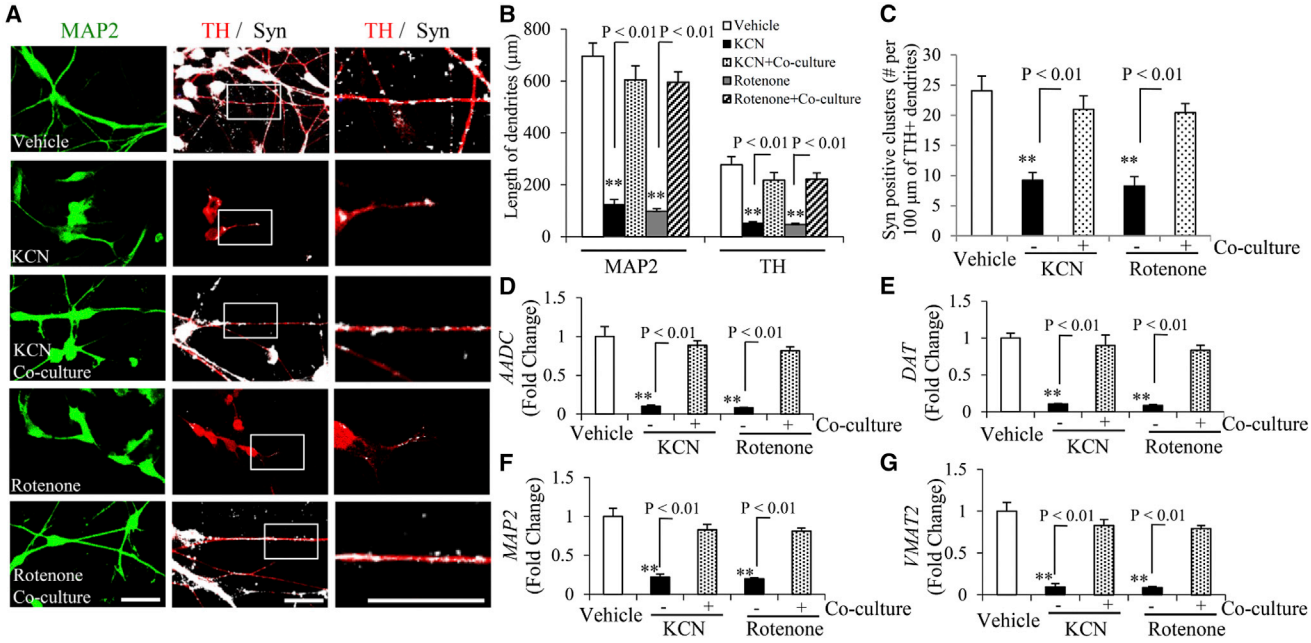

Figure 2. Astrocyte Co-culture Rescues Differentiation of hiPSC Line-Induced Human DA Neurons under KCN or Rotenone Treatment

(A) Representative images for immunostaining of MAP2 (green), TH (red), and Syn (white, color changed from far red) in induced DA neurons treated with KCN or rotenone with or without astrocyte co-culture. Scale bars, 25 μm.

(B) Quantification of neuronal process length of MAP2-positive neurons and TH-positive DA neurons using NIH ImageJ program.

(C) Quantification of numbers of Syn-positive clusters along the branches of hiPSC-derived DA neurons (TH-positive dendrites).

(D–G) Quantitative real-time PCR results of the indicated gene expression levels of *AADC* (D), *DAT* (E), *VMAT2* (G), and *MAP2* (F) in DA neurons with (+) or without (−) co-culture of astrocytes in the presence of vehicle, KCN, or rotenone.

Scale bars, 25 μm in (A). For (B)–(G), **p < 0.01 versus the vehicle group. Statistical analysis was performed using StatView software (SAS Institute, v.5.0.1). One-way ANOVA was used for repeated-measure analysis, followed by Fisher's protected least significant difference for post hoc comparisons. Data are presented as means ± SEM. n = 3 independent experiments, with 12–13 cells quantified per experiment in (B) and (C). n = 3 independent experiments in (D)–(G).

transporter 2 (*VMAT2*), and the marker for mature neurons, *microtubule-associated protein 2* (*MAP2*), were markedly elevated with astroglia co-culture (Figures 2D–2G). These results indicate that co-culture with astrocytes restores DA neuronal differentiation ability and synaptogenesis by improving mitochondrial function. Given that soma size is an important index for neuronal morphology and development, we further analyzed soma size of DA neurons in the aforementioned treatments. No significant changes in soma size of DA neurons were observed between DA neurons with and without astrocyte co-culture exposed to KCN or rotenone (data not shown).

Co-culture with Astrocytes Rescues Mitochondrial Defects in hiPSC-Differentiated DA Neurons

To further determine the effect of astroglial co-culture on neuronal mitochondrial functions, we evaluated the activity of mitochondrial complexes I and IV (key respiratory chain enzymes), ATP levels, and mitochondrial reactive oxygen species (ROS) levels. Co-culture with astrocytes rescued KCN or rotenone-induced mitochondrial dysfunction as shown by increased complex IV and I activities and ATP levels in DA neurons (Figures 3A–3C). Furthermore, in the presence of astrocytes, mitochondrial ROS levels evaluated by MitoSOX staining intensity in TH+ neuronal terminals (Figures 3D and 3E) and intracellular ROS levels measured by highly specific electron paramagnetic resonance (EPR) spectroscopy (Figures 3F and 3G) were both significantly diminished in DA neurons exposed to KCN or rotenone. These results demonstrate that astroglial co-culture rescues mitochondrial respiratory function defects and eliminates ROS overproduction and accumulation during differentiation of hiPSCs into DA neurons.

Co-culture with Astrocytes Protects against Mitochondria Toxin-Induced Alterations in Mitochondrial Morphology and Mobility in hiPSC-Differentiated DA Neurons

Finally, we investigated mitochondrial morphology and mobility in the processes of hiPSC-differentiated DA

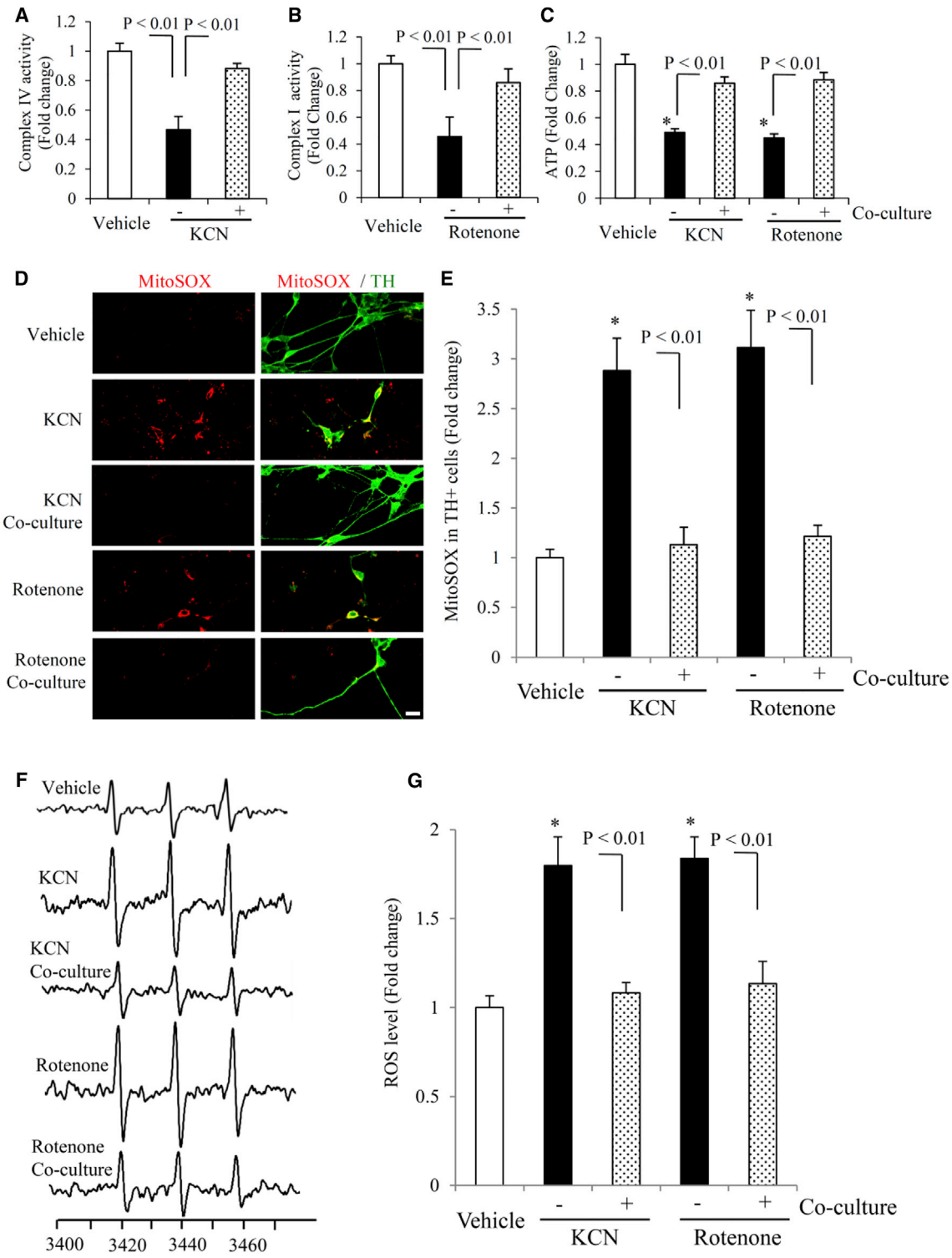

Figure 3. Effect of Astrocyte Co-culture on Mitochondrial Functions in hiPSC Line-Induced Human DA Neurons under KCN or Rotenone Treatment

(A–C) Complex IV (A) and I (B) activity and ATP levels (C) were determined in hiPSC-derived DA neurons treated with KCN or rotenone with or without astrocyte co-culture. Data are expressed as fold change relative to the vehicle group in (A)–(C) (n = 3 independent experiments; mean ± SEM).

(legend continued on next page)

neurons. Cumulative distribution data in Figure 4A clearly demonstrate that astroglial co-culture increases the percentage of long mitochondria in hiPSC-differentiated DA neurons under KCN or rotenone treatment. Mitochondrial travel distance and velocity were significantly increased in DA neurons co-cultured with astrocytes compared with DA neurons without astrocytes in the presence of KCN or rotenone (Figures 4B and 4C). Similarly, the percentages of anterograde, retrograde, and movable mitochondria were all increased (Figures 4D and 4E), whereas the percentage of stationary mitochondria was decreased in neurons cultured with astrocytes (Figure 4D). Representative kymograph images revealed more movable mitochondria in the neuronal processes of KCN- and rotenone-treated DA neurons with astroglial co-culture (Figure 4F). Video recorded from living mitochondrial images revealed a significant improvement in mitochondrial movement speed and travel distance with astrocyte co-culture (Movie S1). Collectively, our results indicate that astrocytes reverse mitochondrial morphological and dynamic defects in hiPSC-derived DA neurons insulted by mitochondrial toxins.

DISCUSSION

Accumulating evidence now suggests that astrocytes are key neuromodulators that actively communicate/cross talk with neurons during different phases of neurodevelopment (Kettenmann and Verkhratsky, 2008; Sofroniew and Vinters, 2010). Astroglial cells are involved in many cellular functions, including providing trophic support for neurons, neurotransmission, metabolite and electrolyte homeostasis, cell signaling, inflammation, and synapse modulation in the CNS (Rouach et al., 2008). Loss of normal homeostatic function, toxic stimulation, or a combination of both activates astrocytes, contributing to the neuropathology of neurodegenerative diseases (Allaman et al., 2011; Booth et al., 2017).

Recently, several studies have demonstrated that astrocytes generated from hiPSCs mimic normal development and functions *in vivo* (Ruiz et al., 2010; Shaltouki et al., 2013). Exposure to FGF was sufficient to induce a mature quiescent spinal cord astrocyte phenotype (Roybon et al., 2013). CNTF has been shown to direct differentiation of precursor cells into astrocytes while inhibiting neuronal differentiation (Bonni et al., 1997). By application of FGF at the astroglial progenitor stage and CNTF at the late stage, we directed hiPSCs into mature GFAP-positive astrocytes 9 months after astroglial induction.

In the CNS, astrocytes have been widely shown to protect neurons from oxidative insults (Shih et al., 2003; Sofroniew and Vinters, 2010). The co-culture system offers a model for mimicking the *in vivo* environment for detailed study of the astrocyte-neuron coordination relationship. In this study, using transwell inserts plated with mature astrocytes, mitochondrial development and differential ability were restored in DA neurons with mitochondrial respiratory inhibitor insult. Similarly, incubation of astrocyte conditioned medium protects against mitochondrial toxin-induced defects in mitochondrial function, differentiation, and synaptogenesis in hiPSC line-induced human DA neurons (Figure S2). These findings indicate that astrocytes are of key importance in modulating neuronal mitochondrial dysfunction induced by mitochondrial insults *in vivo*.

Mitochondria, highly dynamic organelles and the primary energy-generating system, contain complex structures involved in multiple processes, including energy metabolism, ROS generation, and mitochondrial dynamics and distribution. Mitochondrial defects occur in a wide variety of degenerative diseases such as aging, mal-neurodevelopment, and neurodegenerative diseases (Mattson et al., 2008). Excess mitochondrial ROS in NPCs could lead to mitochondrial dysfunctions, resulting in failure of DA neurons to differentiate (Fang et al., 2016a). Since astrocytes are potent scavengers of ROS, neurons are damaged by oxidative stress triggered by the impaired redox scavenging ability of dysfunctional astrocytes (Drukarch et al., 1998). Indeed, astroglial-neuronal co-culture reduced intracellular mitochondrial ROS levels and restored mitochondrial function along with differentiation of DA neurons insulted by mitochondrial toxin, suggesting the protective effect of astrocytes on DA neuronal function and differentiation is, at least in part, via suppressing ROS to stabilize mitochondrial functions.

Mitochondrial ROS is a strong stimulus, which activates many signal pathways and transcription factors, including

(D and E) Mitochondrial ROS levels were measured by MitoSOX staining. Representative images for MitoSOX staining for hiPSC-derived DA neurons with the above treatments are shown in (D), and quantification of MitoSOX staining intensity is shown in (E) (n = 3 independent experiments; mean ± SEM, with five cells quantified per experiment). Scale bars, 10 μm in (D).

(F and G) Assessment of intracellular ROS levels measured by EPR spectroscopy. Representative images for EPR are shown in (F), and quantifications are shown in (G) (n = 3 independent experiments; mean ± SEM).

*$p < 0.05$ versus the vehicle group (C, E, and G). Statistical analysis was performed using Statview software (SAS Institute, Version 5.0.1). One-way ANOVA was used for repeated measure analysis, followed by Fisher's protected least significant difference for post hoc comparisons (A–C, E, and G).

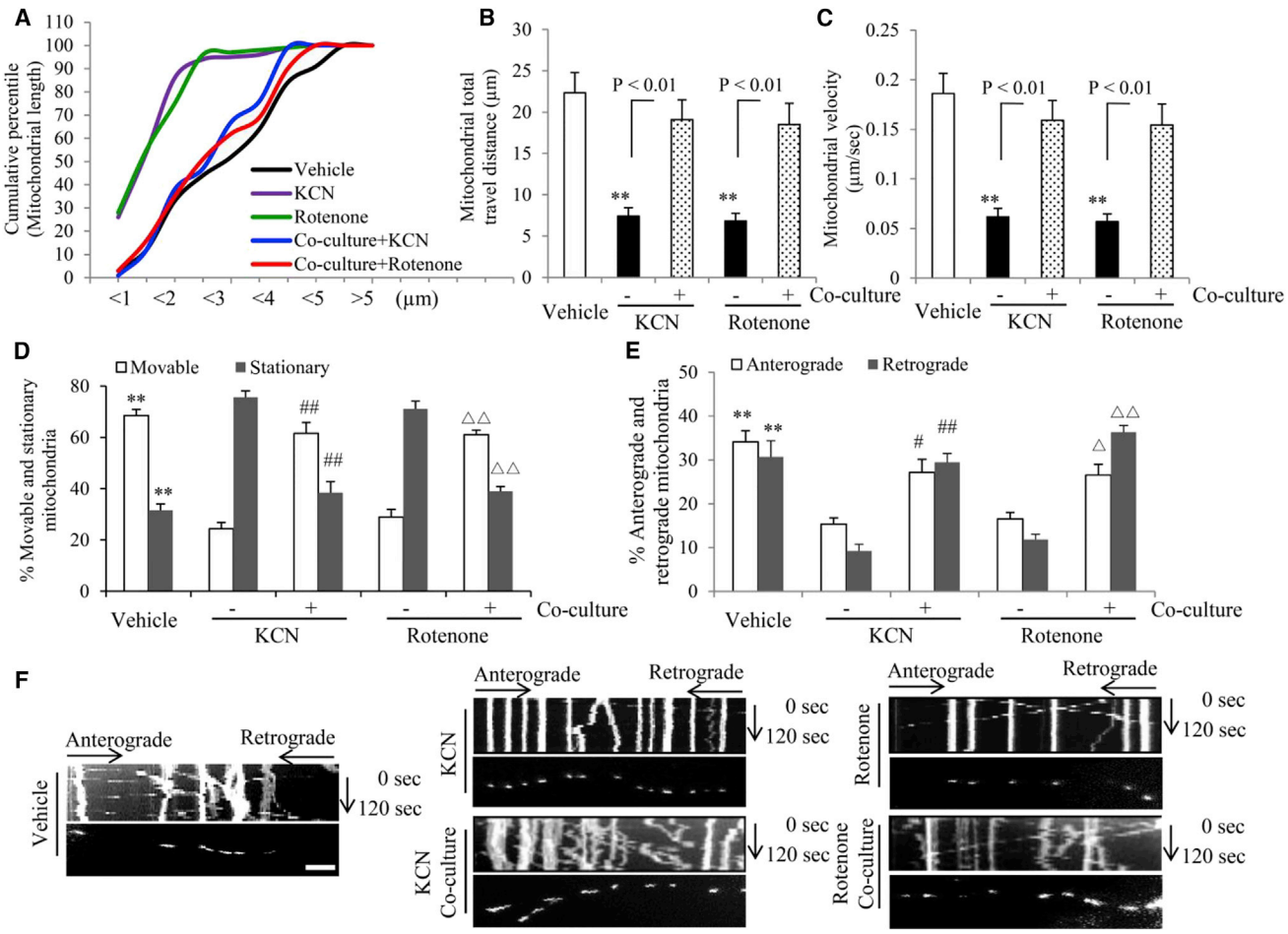

Figure 4. Effect of Astrocyte Co-culture on Mitochondrial Dynamic Parameters in hiPSC-Derived DA Neurons under KCN or Rotenone Treatment

(A) Cumulative distribution data showed increases in the numbers of long mitochondria in hiPSC-derived DA neurons treated with KCN or rotenone with or without astrocyte co-culture.

(B and C) Average mitochondrial travel distance (B) and mitochondrial travel velocity (C) were calculated. Longer mitochondrial travel distance and higher mitochondrial travel velocity were obtained from DA neurons with astrocyte co-culture. $^{**}p < 0.01$ versus the vehicle group.

(D and E) Higher percentage of movable and lower percentage of stationary (D) and more anterograde and retrograde movable mitochondria (E) in DA neurons with astrocyte co-culture. n = 3 independent experiments; mean ± SEM, with 10 mitochondrial movements quantified per experiment in (B)–(E). $^{**}p < 0.01$ versus the open and gray bars in the KCN- and rotenone-treated groups without astrocyte (−), respectively. $^{\#}p < 0.05$ and $^{\#\#}p < 0.01$ versus the open and gray bars in the KCN-treated groups (−), respectively. $^{\triangle}p < 0.05$ and $^{\triangle\triangle}p < 0.01$ versus the open and gray bars in the rotenone-treated groups (−), respectively. Statistical analysis was performed using Statview software (SAS Institute, Version 5.0.1). One-way ANOVA was used for repeated measure analysis, followed by Fisher's protected least significant difference for post hoc comparisons (B–E).

(F) Kymographs generated from live-imaging movies represent hiPSC-derived DA neurons cultured with above treatments. In the kymographs, the x axis is mitochondrial position and the y axis represents the time lapse of 0–120 s. Vertical white lines represent stationary mitochondria and diagonal lines represent moving mitochondria. Anterograde movements are from left to right and retrograde movements are from right to left. Scale bar, 10 μm.

nuclear factor κB and p38 or ERK mitogen-activated protein (MAP) kinases. Oxidative stress-mediated activation of p38 MAP kinase contributes to aberrant axonal mitochondrial transport and aberrant mitochondrial dynamics and function (Yu et al., 2016, 2017). Disruption of ERK MAP kinase signaling perturbs the balance of mitochondrial dynamics via increased mitochondrial fission protein Dlp1 expression in Alzheimer's disease trans-mitochondrial "cybrid" (cytoplasmic hybrid) neuronal cells (Gan et al., 2014, 2015). Our most recent study demonstrated the link of

mitochondrial ROS to mitochondrial clearance through the PINK1-mediated autophagy pathway to maintain homeostasis of mitochondria (Du et al., 2017). Thus, mitochondrial ROS-initiated signals may contribute importantly to the astrocyte-involved DA neuronal maturation and synaptogenesis.

Mitochondria continuously undergo fission and fusion cycles. During DA neuronal differentiation, mitochondria favor the fusion process (Fang et al., 2016a). The fission and fusion balance is maintained via quality control of mitochondrial proteins, such as Drp1, a key mitochondrial fission protein found to be indispensable in somatic cell reprogramming to pluripotency (Vazquez-Martin et al., 2012), and fusion proteins. Importantly, mitochondrial trafficking regulator Miro1 (Mitochondrial Rho GTPase 1), a key factor in normal embryonic development, is also involved in the differentiation of iPSCs (Chen et al., 2003; Yamaoka et al., 2011).

In addition, multiple trophic factors as bFGF, BDNF, GDNF, and NGF, derived from astrocytes, have been implicated in regulating mesencephalic DA neuronal survival, differentiation, and synaptic plasticity *in vitro* and *in vivo* (Liu et al., 2015; Yang et al., 2014). These tropic factors are potentially important for the astrocyte-involved mitochondrial improvement, synaptogenesis, and development of DA.

Endoplasmic reticulum (ER) stress results in accumulation of unfolded or misfolded proteins in the ER lumen. ER and mitochondria form networks essential to maintain cellular homeostasis; therefore, ER stress perturbs mitochondrial function (Malhotra and Kaufman, 2011). Under chronic KCN and rotenone treatments, the protein disulfide isomerase, a stress protein abundant in ER, and the ER chaperone glucose-regulated protein 78 were elevated in the DA neurons (Figure S3). Notably, co-culture with astrocytes almost abolished KCN- or rotenone-mediated upregulation of these ER stress markers. These results suggest a possible link of mitochondrial dysfunction to ER stress via astrocytes, contributing to the normal differentiation and synaptogenesis in DA neurons.

Mitochondrial dysfunction and oxidative stress play a major role in the pathogenesis of PD. Deficiency of mitochondrial complex I of the respiratory chain has long been implicated in the cause of the degeneration of PD-affected neurons (Mizuno et al., 1998). In addition, combined decreased complex I and IV activity was seen in the platelet mitochondria of PD (Benecke et al., 1993) and 1-methyl-4-phenyl 1,2,3,6-tetrahydropyridine (MPTP)- or 6-hydroxydopamine-induced animal models of PD (Desai et al., 1996; Glinka and Youdim, 1995). Here, we induced DA neuron differentiation by co-culture with mature astrocytes to mimic the *in vivo* neuronal-astroglial interaction environment. Therefore, evaluation of the consequences of mitochondrial toxin-mediated inhibition of mitochondrial respiratory function via complex I or IV on dopamine neurons holds a potential significance for the pathogenesis of DA degeneration relevant to the PD pathology.

In summary, we have clearly demonstrated the direct role of mitochondria in DA neuron maturation and an active astrocyte-neuron coordination relationship. The present model provides an approach for the study of abnormal mitochondrial structure, function, and dynamics in the pathogenesis of neurodegenerative diseases and, importantly, an approach for therapeutic discovery in neurodegenerative diseases such as PD.

EXPERIMENTAL PROCEDURES

hiPSC Culture

Bone marrow 2-3 (BM2-3) from hiPSCs passaged 16–20 times were obtained from Dr. Sunita L. D'Souza. This BM2-3 iPSC line was derived from the bone marrow of a clinically normal human subject and verified by fluorescence *in situ* hybridization test showing 46, XX. Cytogenetic analysis of cultured human stem cells revealed a normal female karyotype. This analysis did not show any evidence of a clinically significant numerical or structural chromosomal abnormality (Fang et al., 2016a). Cells were maintained under feeder-free conditions using Matrigel (BD Biosciences)-coated six-well tissue culture plates in Essential 8 Medium (Life Technologies), supplemented with 10 μM ROCK inhibitor Y27632 (Life Technologies). Cells were routinely passaged as small clumps using a previously described EDTA method (Fang et al., 2016a).

Neuron and Astrocyte Co-culture System

For co-culture experiments, 2.5×10^4 astrocytes per well were first seeded on the 12-well transwell cell culture insert system (pore size 0.4 μm; Falcon, USA) and allowed to grow for 5 days. On day 6, astroglial medium was changed to DA neuronal differentiation medium. After 2 days, the transwell inserts were placed into wells of NPCs during induction, and future experiments were conducted 2 days after the insertion of the astroglial transwells (Figure 1A).

SUPPLEMENTAL INFORMATION

Supplemental Information includes Supplemental Experimental Procedures, three figures, and one movie and can be found with this article online at https://doi.org/10.1016/j.stemcr.2017.12.021.

AUTHOR CONTRIBUTIONS

S.S.Y. initiated, directed, designed, and supervised research and wrote the paper. F.D. and Q.Y. developed the concept and designed research. F.D., Q.Y., A.C., and D.C. conducted experiments, analyzed data, and wrote the paper.

ACKNOWLEDGMENTS

We thank Dr. Sunita L. D'Souza (Department of Gene and Cell Medicine and Black Family Stem Cell Institute and Department

of Developmental and Regenerative Biology, Icahn School of Medicine at Mount Sinai, NY, USA) for providing iPSCs. This study was supported by grants from the NIH (R37AG037319, R01AG044793, R01AG05341, and R01NS089116). We thank Dr. Justin T. Douglas for assistance using the EPR instrument. The EPR instrumentation was provided by NSF Chemical Instrumentation Grant (no. 0946883).

Received: August 1, 2017
Revised: December 27, 2017
Accepted: December 28, 2017
Published: January 25, 2018

REFERENCES

Allaman, I., Belanger, M., and Magistretti, P.J. (2011). Astrocyte-neuron metabolic relationships: for better and for worse. Trends Neurosci. *34*, 76–87.

Benecke, R., Strumper, P., and Weiss, H. (1993). Electron transfer complexes I and IV of platelets are abnormal in Parkinson's disease but normal in Parkinson-plus syndromes. Brain *116* (Pt 6), 1451–1463.

Bonni, A., Sun, Y., Nadal-Vicens, M., Bhatt, A., Frank, D.A., Rozovsky, I., Stahl, N., Yancopoulos, G.D., and Greenberg, M.E. (1997). Regulation of gliogenesis in the central nervous system by the JAK-STAT signaling pathway. Science *278*, 477–483.

Booth, H.D.E., Hirst, W.D., and Wade-Martins, R. (2017). The role of astrocyte dysfunction in Parkinson's Disease pathogenesis. Trends Neurosci. *40*, 358–370.

Chen, H., Detmer, S.A., Ewald, A.J., Griffin, E.E., Fraser, S.E., and Chan, D.C. (2003). Mitofusins Mfn1 and Mfn2 coordinately regulate mitochondrial fusion and are essential for embryonic development. J. Cell Biol. *160*, 189–200.

Desai, V.G., Feuers, R.J., Hart, R.W., and Ali, S.F. (1996). MPP(+)-induced neurotoxicity in mouse is age-dependent: evidenced by the selective inhibition of complexes of electron transport. Brain Res. *715*, 1–8.

Drukarch, B., Schepens, E., Stoof, J.C., Langeveld, C.H., and Van Muiswinkel, F.L. (1998). Astrocyte-enhanced neuronal survival is mediated by scavenging of extracellular reactive oxygen species. Free Radic. Biol. Med. *25*, 217–220.

Du, F., Yu, Q., Yan, S., Hu, G., Lue, L.F., Walker, D.G., Wu, L., Yan, S.F., Tieu, K., and Yan, S.S. (2017). PINK1 signalling rescues amyloid pathology and mitochondrial dysfunction in Alzheimer's disease. Brain *140*, 3233–3251.

Fang, D., Qing, Y., Yan, S., Chen, D., and Yan, S.S. (2016a). Development and dynamic regulation of mitochondrial network in human midbrain dopaminergic neurons differentiated from iPSCs. Stem Cell Reports *7*, 678–692.

Fang, D., Yan, S., Yu, Q., Chen, D., and Yan, S.S. (2016b). Mfn2 is required for mitochondrial development and synapse formation in human induced pluripotent stem Cells/hiPSC derived cortical neurons. Sci. Rep. *6*, 31462.

Gan, X., Huang, S., Wu, L., Wang, Y., Hu, G., Li, G., Zhang, H., Yu, H., Swerdlow, R.H., Chen, J.X., et al. (2014). Inhibition of ERK-DLP1 signaling and mitochondrial division alleviates mitochondrial dysfunction in Alzheimer's disease cybrid cell. Biochim. Biophys. Acta *1842*, 220–231.

Gan, X., Huang, S., Yu, Q., Yu, H., and Yan, S.S. (2015). Blockade of Drp1 rescues oxidative stress-induced osteoblast dysfunction. Biochem. Biophys. Res. Commun. *468*, 719–725.

Glinka, Y.Y., and Youdim, M.B. (1995). Inhibition of mitochondrial complexes I and IV by 6-hydroxydopamine. Eur. J. Pharmacol. *292*, 329–332.

Kettenmann, H., and Verkhratsky, A. (2008). Neuroglia: the 150 years after. Trends Neurosci. *31*, 653–659.

Kriks, S., Shim, J.W., Piao, J., Ganat, Y.M., Wakeman, D.R., Xie, Z., Carrillo-Reid, L., Auyeung, G., Antonacci, C., Buch, A., et al. (2011). Dopamine neurons derived from human ES cells efficiently engraft in animal models of Parkinson's disease. Nature *480*, 547–551.

Lancaster, M.A., and Knoblich, J.A. (2014). Organogenesis in a dish: modeling development and disease using organoid technologies. Science *345*, 1247125.

Liu, H., Tang, X., and Gong, L. (2015). Mesencephalic astrocyte-derived neurotrophic factor and cerebral dopamine neurotrophic factor: new endoplasmic reticulum stress response proteins. Eur. J. Pharmacol. *750*, 118–122.

Lo, E.H. (2010). Degeneration and repair in central nervous system disease. Nat. Med. *16*, 1205–1209.

Malhotra, J.D., and Kaufman, R.J. (2011). ER stress and its functional link to mitochondria: role in cell survival and death. Cold Spring Harb. Perspect. Biol. *3*, a004424.

Maragakis, N.J., and Rothstein, J.D. (2006). Mechanisms of disease: astrocytes in neurodegenerative disease. Nat. Clin. Pract. Neurol. *2*, 679–689.

Maroof, A.M., Keros, S., Tyson, J.A., Ying, S.W., Ganat, Y.M., Merkle, F.T., Liu, B., Goulburn, A., Stanley, E.G., Elefanty, A.G., et al. (2013). Directed differentiation and functional maturation of cortical interneurons from human embryonic stem cells. Cell Stem Cell *12*, 559–572.

Mattson, M.P., Gleichmann, M., and Cheng, A. (2008). Mitochondria in neuroplasticity and neurological disorders. Neuron *60*, 748–766.

Mizuno, Y., Yoshino, H., Ikebe, S., Hattori, N., Kobayashi, T., Shimoda-Matsubayashi, S., Matsumine, H., and Kondo, T. (1998). Mitochondrial dysfunction in Parkinson's disease. Ann. Neurol. *44*, S99–S109.

Rouach, N., Koulakoff, A., Abudara, V., Willecke, K., and Giaume, C. (2008). Astroglial metabolic networks sustain hippocampal synaptic transmission. Science *322*, 1551–1555.

Roybon, L., Lamas, N.J., Garcia, A.D., Yang, E.J., Sattler, R., Lewis, V.J., Kim, Y.A., Kachel, C.A., Rothstein, J.D., Przedborski, S., et al. (2013). Human stem cell-derived spinal cord astrocytes with defined mature or reactive phenotypes. Cell Rep. *4*, 1035–1048.

Ruiz, S., Brennand, K., Panopoulos, A.D., Herrerias, A., Gage, F.H., and Izpisua-Belmonte, J.C. (2010). High-efficient generation of induced pluripotent stem cells from human astrocytes. PLoS One *5*, e15526.

Shaltouki, A., Peng, J., Liu, Q., Rao, M.S., and Zeng, X. (2013). Efficient generation of astrocytes from human pluripotent stem cells in defined conditions. Stem Cells *31*, 941–952.

Shih, A.Y., Johnson, D.A., Wong, G., Kraft, A.D., Jiang, L., Erb, H., Johnson, J.A., and Murphy, T.H. (2003). Coordinate regulation of glutathione biosynthesis and release by Nrf2-expressing glia potently protects neurons from oxidative stress. J. Neurosci. *23*, 3394–3406.

Sofroniew, M.V., and Vinters, H.V. (2010). Astrocytes: biology and pathology. Acta Neuropathol. *119*, 7–35.

Vazquez-Martin, A., Cufi, S., Corominas-Faja, B., Oliveras-Ferraros, C., Vellon, L., and Menendez, J.A. (2012). Mitochondrial fusion by pharmacological manipulation impedes somatic cell reprogramming to pluripotency: new insight into the role of mitophagy in cell stemness. Aging *4*, 393–401.

Yamaoka, S., Nakajima, M., Fujimoto, M., and Tsutsumi, N. (2011). MIRO1 influences the morphology and intracellular distribution of mitochondria during embryonic cell division in *Arabidopsis*. Plant Cell Rep. *30*, 239–244.

Yang, F., Liu, Y., Tu, J., Wan, J., Zhang, J., Wu, B., Chen, S., Zhou, J., Mu, Y., and Wang, L. (2014). Activated astrocytes enhance the dopaminergic differentiation of stem cells and promote brain repair through bFGF. Nat. Commun. *5*, 5627.

Yu, Q., Du, F., Douglas, J.T., Yu, H., Yan, S.S., and Yan, S.F. (2017). Mitochondrial dysfunction triggers synaptic deficits via activation of p38 MAP kinase signaling in differentiated Alzheimer's Disease trans-mitochondrial cybrid cells. J. Alzheimers Dis. *59*, 223–239.

Yu, Q., Fang, D., Swerdlow, R.H., Yu, H., Chen, J.X., and Yan, S.S. (2016). Antioxidants rescue mitochondrial transport in differentiated Alzheimer's Disease trans-mitochondrial cybrid cells. J. Alzheimers Dis. *54*, 679–690.

Stem Cell Reports, Volume *10*

Supplemental Information

Astrocytes Attenuate Mitochondrial Dysfunctions in Human Dopaminergic Neurons Derived from iPSC

Fang Du, Qing Yu, Allen Chen, Doris Chen, and Shirley ShiDu Yan

Supplemental Figures and Legends

Supplementary Figure S1.

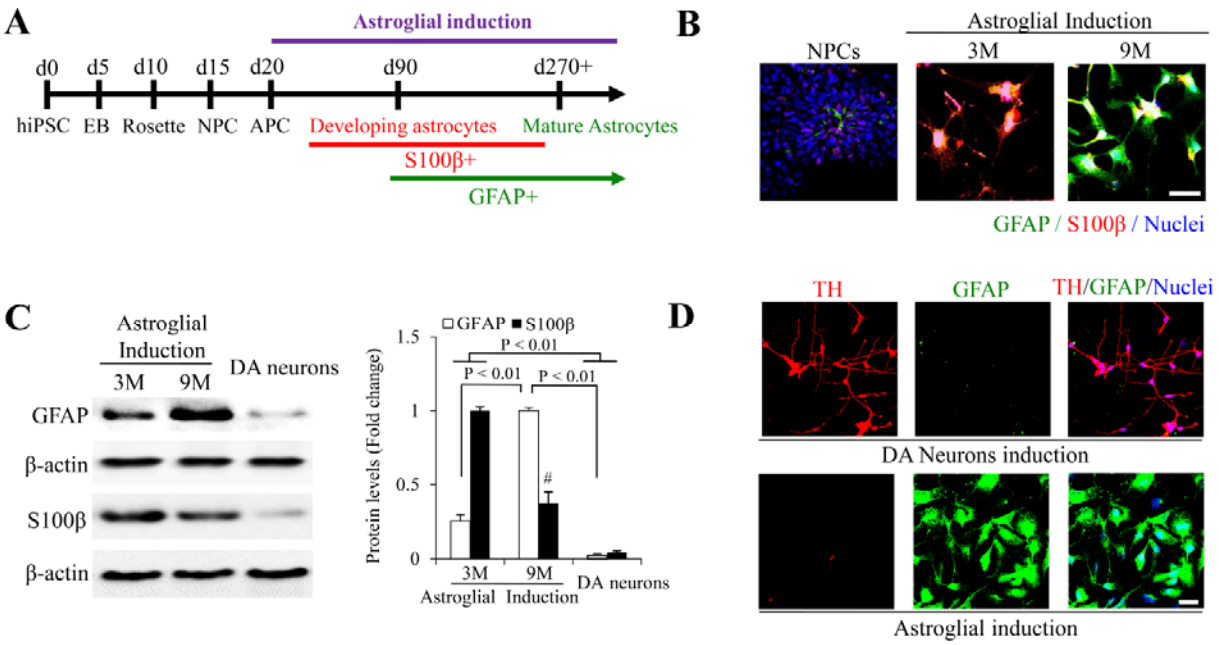

Figure S1 (Related to Figure 1: Differentiation and development of hiPSC line-induced human astrocytes). Differentiation of hiPSCs BM2-3 lines into astrocytes. (**A**) A schematic representation of processes of differentiation of human bone marrow fibroblast-derived hiPSCs BM2-3 into astroglial progenitors (S100β+) and mature astrocytes (GFAP+). (**B**) Immunocytochemistry of GFAP (Marker for definitive astrocytes, green) and S100β (Marker for astroglial progenitor, red) in neural progenitor cells (NPCs), astroglial progenitor (3 months with astroglial induction) and mature astrocytes (9 months with astroglial induction). Nuclei were stained by DRAQ5 (5 μM, Cell Signaling). Scale bar, 50 μm. (**C**) immunoblotting analyses to detect GFAP and S100β in astroglial and mature astrocytes in comparison with hiPSCs induced DA neurons. #P < 0.05 vs. 3-month astrocytes and DA neurons (Black bars, S100β). (**D**) Immunocytochemistry of TH (red) and GFAP (green) in mature DA neurons (up panel) and

mature astrocytes (bottom panel). Nuclei were stained by DRAQ5. Scale bar, 50 μm. For (**C**), statistical analysis was performed using Statview software (SAS Institute, Version 5.0.1). One-way ANOVA was used for repeated measure analysis, followed by Fisher's protected least significant difference for post hoc comparisons. Data are presented as mean ± SEM. n = 3 independent experiments.

Supplementary Figure S2.

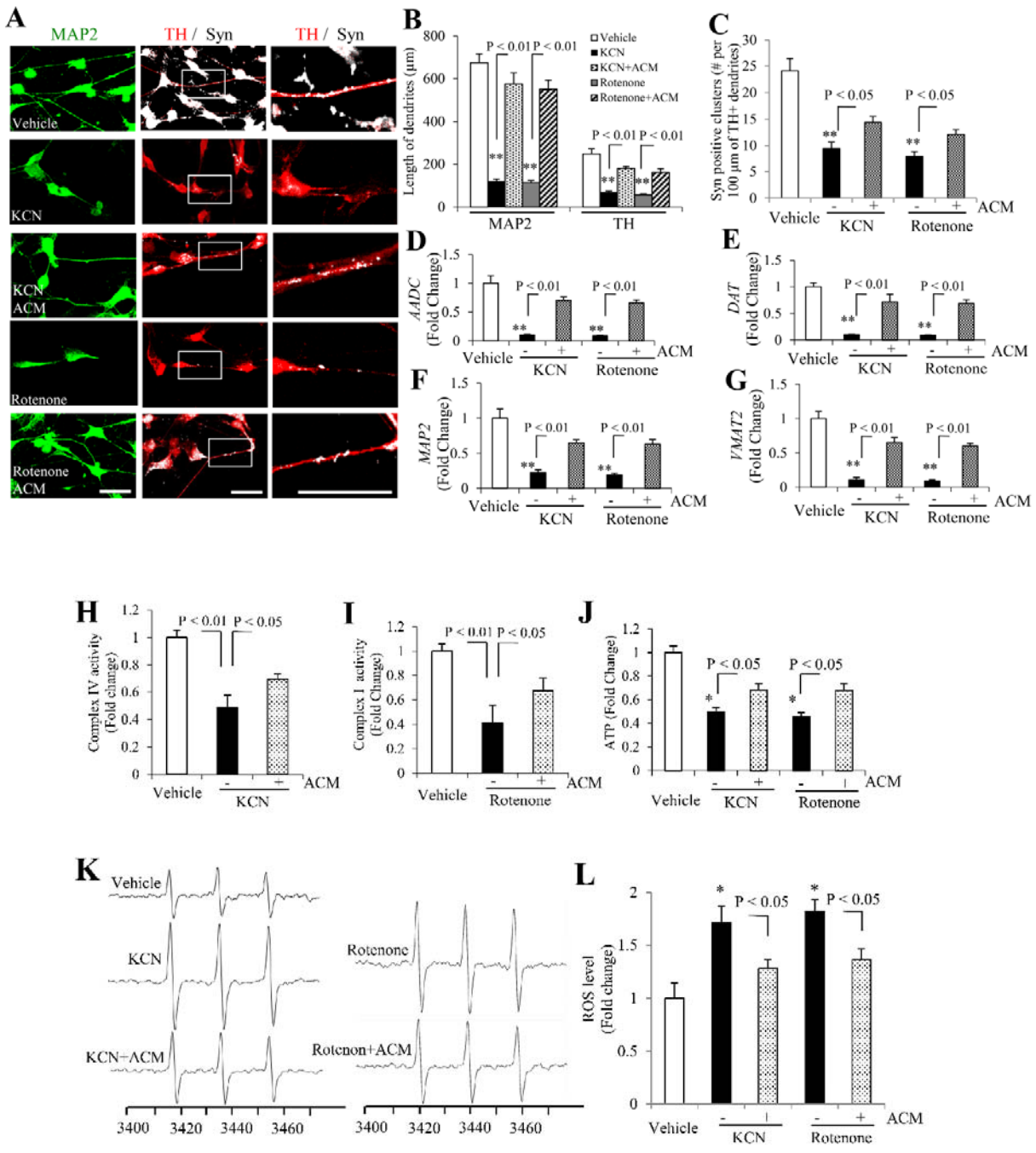

Figure S2 (Related to Figure 2: Astrocyte co-culture rescues differentiation of hiPSC line-induced human DA neurons under KCN or rotenone treatment, and Figure 3. Effect of astrocyte co-culture on mitochondrial functions in hiPSC line-induced human DA neurons under KCN or rotenone treatment). Astrocyte conditioned medium (ACM) rescues differentiation impairment and mitochondrial dysfunction of hiPSC line-induced human DA neurons under KCN or rotenone treatment. The effects of ACM on the differentiation ability and mitochondrial functions in hiPSC line-induced human DA neurons under KCN or rotenone treatment were also observed and compared to the co-culture system. (**A**) Representative images for immunostaining of MAP2 (green), TH (red) and Syn (White, color changed from far red) in induced DA neurons treated with KCN or rotenone with or without ACM cotreatment. (**B**) Quantification of neuronal process length of MAP2-positive neurons and TH-positive DA neurons using NIH Image J program. (**C**) Quantification of numbers of Syn-positive clusters along the branches of hiPSC-derived DA neurons (TH-positive dendrities). (**D-G**) Quantitative RT-PCR results of the gene expression in DA neurons with the above treatments. Scale bars = 25 μm in **A**. Complex IV (**H**) and I (**I**) activity and ATP levels (**J**) were determined in hiPSC-derived DA neurons treated with KCN or rotenone with or without ACM cotreatment. (**K-L**) Assessment of intracellular ROS levels measured by EPR spectroscopy. Representative images for EPR are shown in **K**, and quantifications are shown in **L**. For (**B-J** and **L**), statistical analysis was performed using Statview software (SAS Institute, Version 5.0.1). One-way ANOVA was used for repeated measure analysis, followed by Fisher's protected least significant difference for post hoc comparisons. Data are presented as mean ± SEM. n = 3 independent experiments, with 12 cells quantified per experiment in (**B-C**). n = 3 independent experiments in **D-J** and **L**; mean ± SEM.

Supplementary Figure S3.

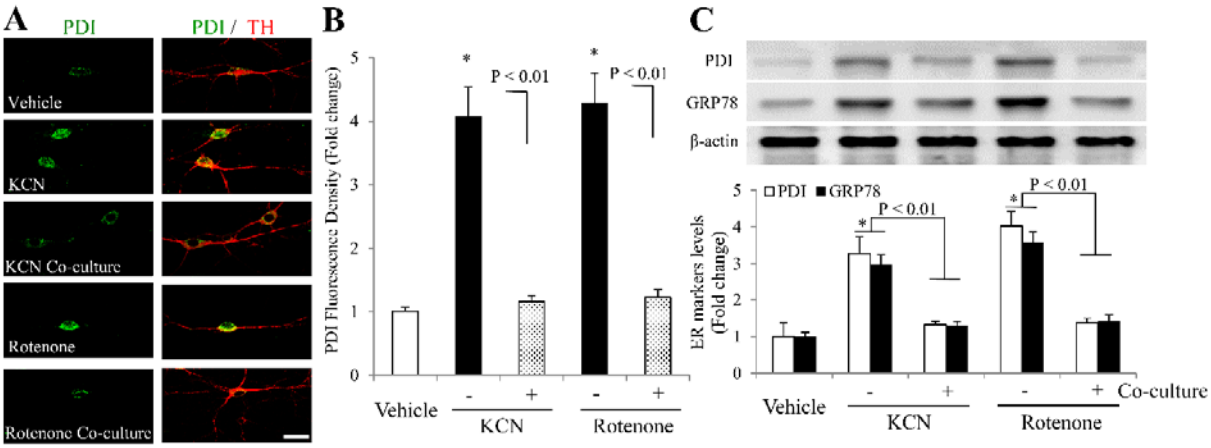

Figure S3 (Related to Figure 3. Effect of astrocyte co-culture on mitochondrial functions in hiPSC line-induced human DA neurons under KCN or rotenone treatment). Astrocyte co-culture rescues ER stress in differentiation of hiPSC line-induced human DA neurons under KCN or rotenone treatment. Besides mitochondrial dysfunction (**Figure 3**), long-term application of low doses of KCN and rotenone also induced ER stress in hiPSC-induced DA neurons, whereas astrocyte co-culture rescued both mitochondrial dysfunction (**Figure 3**) and ER stress. (**A**) Immunocytochemistry of a luminal endoplasmic reticulum (ER) protein, PDI (Protein disulfide isomerase) and TH (red) in mature DA neurons, and (**B**) bar graph shows the quantification of fluorescence density of PDI in DA neurons using NIH Image J program. (**C**) Immunoblotting analyses to detect PDI and GRP78 (Glucose-regulated protein 78, used as a marker of ER stress) in hiPSC-induced DA neurons. *P < 0.01 vs. vehicle group (**B-C**).

Supplementary Video S1. (Related to Figures 4B-F). Mitochondrial movement in the neurites of hiPSC-derived DA neurons with different treatments. Videos S1A-E: mitochondrial movement in the neurites of hiPSC-derived DA neurons with vehicle treatment

(**Video S1A**); KCN treatment (**Video S1B**); rotenone treatment (**Video S1C**), and KCN (**Video S1D**) or rotenone (**Video S1E**) treatment with astroglial co-culture.

Supplemental Experimental Procedures

Formation of embryoid bodies and induction of rosette

Feeder-free iPSCs were dissociated with TryplE and seeded onto AggreWell™800 plate (10,000 cells per embryoid body; Stem Cell Technologies) in E8 media supplemented with 10 μM ROCK inhibitor Y27632 for the first 24 h; we changed 75% of the media daily with STEMdiff™ Neural Induction Medium (NIM, Stem Cell Technologies). Embryoid bodies were harvested after 5 days and plated onto poly-L-ornithine/laminin (PLO/L, Sigma) coated plates. 1-2 day(s) after attachment, prominent neural rosette structures were visible inside the attached neural aggregates. Rosettes were formed by cells expressing proteins characteristic of progenitor markers of PAX6 and Ki67 (Fang et al., 2016a; Fang et al., 2016b).

Isolation of stem/progenitor cells and differentiation of DA neurons

We followed the differentiation protocol (Hartfield et al., 2014) with some modifications. Briefly, stem/progenitor cells from neuronal rosette clusters were isolated using Neural Rosette Selection Reagent (Stem Cell Technologies) 5 days after incubation in NIM. Detached cells were collected and plated onto poly l Ornithine/Laminin (PLO/L) coated 6-well plates for Western blot analysis and complex activities measurement (2×10^4 cells per well), 12-well plates for co-culture system (1×10^4 cells per well), or coverslips for immunocytochemistry and electrophysiology (5×10^3 cells per coverslip). Neural progenitor cells (NPCs) were cultured in neural expansion medium (DMEM/F12 supplemented with 1 × B27 and N2 [Life technologies], fibroblast growth factor-8a [FGF8a, 100 ng/ml, Life technologies], sonic hedgehog [SHH C25II,

200 ng/ml, Life technologies]; Heparin [2 μg/ml, Life technologies] and 1× non-essential amino acids [NEAA, Life technologies] for 5 days and finally in DA neuronal differentiation medium (Neurobasal medium supplemented with L-glutamine [2 mM, Life technologies], 1× B27 and N2 supplements, Brain-derived neurotrophic factor [BDNF, 25 ng/ml], glial-derived neurotrophic factor [GDNF, 20 ng/ml], N6,29-O-dibutyryladenosine 39,59-cyclic monophosphate sodium salt [dCAMP, 100 μM; Sigma] and ascorbic acid [200 μM, Sigma]).

Astroglial differentiation

Astroglial progenitors were differentiated from iPSCs as previously described with some modifications (Krencik et al., 2011; Williams et al., 2014). Briefly, iPSCs were first differentiated to rosettes (Day 10). After cultured in neural expansion medium for 5 days (Day 10-15) and another 5 days for astroglial progenitor cells (APCs) differentiation in an astroglial expansion medium (DMEM/F12 supplemented with N2; Heparin [2μg/ml] and 1× NEAA; Day 15-20), the medium was switched to astroglial progenitor media (APM): astroglial expansion medium with the addition of 10 ng/ml EGF (Pepro-Tech) and 10 ng/ml recombinant human FGF2. From Day 21, these APCs were passaged with Accutase (Life technologies) every 14 days, and were plated at a density of 5×10^4 cells per well in astroglial media (AM): APM with the addition of ciliary neurotrophic factor (CNTF). Terminal differentiated astrocytes were derived from 3 months to 9 months by the removal of the growth factors (EGF and FGF2) in AM.

For astroglial conditioned media (ACM) collection, 2.5×10^4 astrocytes per well were first seeded on the PLO/L coated 12-well plate and allowed to grow for 5 days. On day 6, AM was changed to DA neuronal differentiation medium (500 μl). The medium (ACM) was centrifuged to pellet debris and collected every 2 days, and was used to treat NPC and DA neurons, with or without the presence of mitochondrial inhibitor/ toxin (**Figure 1A**).

Immunoblotting analysis

NPCs, DA neurons, astroglial progenitor and astrocytes were washed with ice-cold PBS and proteins extracted with 150μl of lysis buffer. After centrifugation at 12,000 × g for 10 min at 4°C, we collected the supernatant and determined protein concentrations; we boiled 30 μg proteins in protein loading buffer for 5 min, separated the proteins on a 10% SDS polyacrylamide gel, and subsequently transferred to nitrocellulose membranes. Nonspecific binding was inhibited by incubation in TBST (20 mM Tris-buffered saline with 0.1% Tween 20, pH 7.5) containing 5% nonfat dried milk for 1 hour at room temperature. Membranes were incubated with the following primary antibodies: rabbit anti-S100β (1:500, Abcam, ab52642-100), mouse anti-GFAP antibody (1:3000, Cell signaling, #3670), rabbit anti-TH (1:2000, Chemicon, #657012), mouse anti-PDI IgG (1: 10,000, StressGen, # SPA-891) and rabbit anti-GRP78 (1:5000, StressGen, # SPA-826) overnight at 4°C. After three washes with TBST, membranes were incubated for 2 h with horseradish (HRP)-conjugated secondary antibodies (Pierce Chemical Company, USA) and developed using enhanced chemiluminescence (ECL Amersham Biosciences, England). To ensure equal protein loading of the samples, the same membrane was probed with anti-mouse β-actin monoclonal antibody (Sigma-Aldrich, MO) at a 1: 10,000 dilution.

Immunocytochemistry

The induced DA neurons, NPCs, or the astrocytes, were fixed with 4% ice-cold paraformaldehyde for 5 min and then permeabilized with PBS containing 0.1% Triton and 5% goat serum for 1 h followed by incubation with the following primary antibodies: rabbit anti-S100β (1:500, Abcam, ab52642-100) and mouse anti-GFAP antibody (1:3000, Cell signaling, #3670); rabbit anti-TH (1:2000, Chemicon, #657012) and mouse anti-Syn IgG (1:1000,

chemicon, #MAB5258); rabbit anti-TH (1:2000, Chemicon, #657012) and mouse anti-PDI IgG (1:5000, StressGen, # SPA-891); or rabbit anti-MAP2 (1:5000, Thermo Fisher, # PA517646) at 4°C for 16 h. Cells were incubated with Alexa Fluor 488-conjugated goat anti-mouse IgG and 594 goat anti-rabbit IgG (1: 1000, Invitrogen) or anti-rabbit IgG and 488 goat anti-mouse IgG (1: 1000, Invitrogen) for 1 h at room temperature. After washing with PBS, neurons were covered with Vectashield mounting medium (H-1000, Vector Laboratories). Images were acquired (equal exposure for all groups) using confocal microscopy (Leica) and analyzed using the Universal Metamorph Image Program.

We measured synaptic density of cultured neurons by counting the number of synaptophysin-positive clusters in neuronal dendrites and puncta per 100 microns of TH positive dendrite (presented as the number of synaptophysin clusters per 100 microns of dendrite) and calculated by dividing the length of the TH+ dendrites. Soma size analysis of DA neurons was measured in TH-positive neurons from 30 randomly selected fields using ImageJ software.

Real-time PCR measurement

RNA was extracted identified cells by using TRIzol reagents (Invitrogen, Carlsbad, CA, USA) according to the manufacturer's protocol as described in our previous study (Fang et al., 2015). cDNA was directly preformed using TaqMan reverse transcription reagents kit (Applied Biosystems, Foster City, CA, USA). Total RNA (1 μg) was used for the synthesis of cDNA with TaqMan Reverse Transcription Reagents kit (Roche Applied Biosystems). Real time-PCR was performed on an ABI Prism 7900 Sequence Detection System (Applied Biosystems) with TaqMan PCR Master Mix. Semi-quantitative PCR was performed in the GeneAmp PCR System 2720 (Applied Biosystems), and the same volume of reaction products are electrophoresed on an agarose gel. The sequences of the primers were EN1 (Hs00154977_m1, Thermo Fisher), OTX2

(Hs00222238_m1, Thermo Fisher), FOXA2 (Hs00232764_m1, Thermo Fisher), map2 (Hs00258900_m1, Thermo Fisher), DDC (AADC) (Hs01105048_m1, Thermo Fisher), SLC18A2 (VMAT2) (Hs00996835_m1, Thermo Fisher), LMX1A (Hs00892663_m1, Thermo Fisher), SLC6A3 (DAT) (Hs00997374_m1, Thermo Fisher), ZBTB16 (PLzf) (Hs00957433_m1, Thermo Fisher), DACH1 (Hs00362088_m1, Thermo Fisher).

Measurement of respiratory chain complex enzyme activities and ATP levels

Enzyme activities in complex I (NADH-ubiquinonereductase), complex IV (cytochrome c oxidase, CcO), and ATP levels were determined as described previously (Gan et al., 2014a). The reaction was then initiated by the addition of 50 µl of ferrocytochrome substrate solution (0.22 mM) and changes in absorbance of cytochrome c at 550 nm were measured using a Shimadzu (Kyoto, Japan) UV1200 spectrophotometer. Activity is expressed as micromols of cytochrome oxidized per min^{-1} mg^{-1} protein using an extinction coefficient of 18.64 mM^{-1} cm^{-1}.

ATP levels were determined using an ATP Bioluminescence Assay Kit (Roche) following the manufacturer's instructions (Du et al., 2008; Du et al., 2010). Briefly, cells were harvested using the provided lysis buffer, incubated on ice for 15 minutes, and centrifuged at 13,000g for 10 minutes. ATP levels were measured using a Luminescence plate reader (Molecular Devices) with an integration time of 10 seconds.

Determination of mitochondrial ROS generation with MitoSox Red

Differentiated neuronal cells were seeded at low density onto Lab-Tek eight-well chamber slides (10,000 cells /well). Mitochondrial ROS generation was determined using MitoSox Red (Invitrogen), a unique fluorogenic dye highly selective for detection of superoxide production in live cell mitochondria (Gan et al., 2014a; Gan et al., 2014b; Iuso et al., 2006; Polster et al., 2014; Xu and Chisholm, 2014). Cells were incubated with fresh medium containing 2.5 µM MitoSox

for 30 min at 37°C. To detect mitochondrial ROS in DA neurons, cells were fixed and incubated with rabbit anti-TH (1:2000, Chemicon, #657012) at 4°C for 16 h. followed by incubation with Alexa Fluor 488-conjugated goat anti-rabbit IgG (1: 1000, Invitrogen) for 1 h at room temperature. Fluorescence images were acquired on a Leica SP5 confocal microscope and analyzed using Leica LAS AF software (Leica Wetzlar). Excitation wavelengths were 543 nm for MitoSox and 488nm for TH. Fluorescent signals were quantified using NIH Image J software. We used MetaMorph (Molecular Devices) and NIH Image J software for quantification and measurement of fluorescent signals.

Evaluation of intracellular ROS levels

Intracellular ROS levels were accessed by election paramagnetic resonance (EPR) spectroscopy as described in our previous study (Fang et al., 2015; Fang et al., 2016c). CMH (cyclic hydroxylamine 1-hydroxy-3-methoxycarbonyl-2, 2, 5, 5-tetramethyl-pyrrolidine, 100μM) was incubated with cultured cells for 30 min and then washed with cold PBS. The cells were collected and homogenized with 100 μl of PBS for EPR measurement. The EPR spectra were collected, stored, and analyzed with a Bruker EleXsys 540 x-band EPR spectrometer (Billerica, MA) using the Bruker Software Xepr (Billerica, MA).

Axonal mitochondrial trafficking recording and data analysis in differentiated neuronal cells

These recordings were performed using previously reported protocols (Du et al., 2010; Guo et al., 2013). Axonal mitochondria were visualized following transfection with pDsRed2-mito (Clontech) in differentiated neuronal cells using lipofectamine LTX and plus regent (Invitrogen) according to the manufacturer's protocol. Three to four days after transfection, time-lapse recordings of labeled mitochondrial movement were acquired on a Carl Zeiss (Axiovert 200)

microscope with incubation system (PeCon) to maintain differentiated neuronal cells at 37°C during image collection. Collection of image stacks and velocity measurements were made using the AxioVision Software as previously described (Du et al., 2010; Guo et al., 2013). For standard recordings, images of mitochondria in one process per differentiated neuronal cell were collected every 3 s for 2 min. Only the proximal segment of the axon was acquired and recorded.

Mitochondria in each frame of every video recording were individually tracked using AxioVision Software and the average velocity was calculated during the 2-min recording period. The average velocity of every mitochondrion in one measured process in each cell was then averaged to obtain the average velocity for mitochondrial movement per process. In addition, the percentage of movable mitochondria, mitochondrial total traveling distance (total distance traveled irrespective of direction during the recording period), single mitochondrial length and mitochondrial density in each process were all determined according to previous studies with modifications (Gan et al., 2014a; Trimmer and Borland, 2005). Exposure periods (30–50 ms) were kept at a minimum to limit phototoxicity.

Statistical analysis

Statistical analysis was performed using Statview software (SAS Institute, Version 5.0.1). One-way ANOVA or Student's t-test was used for repeated measure analysis, followed by Fisher's protected least significant difference for post hoc comparisons. Data are presented as mean ± SEM. $P < 0.05$ was considered significant.

Supplemental References

Du, H., Guo, L., Fang, F., Chen, D., Sosunov, A.A., McKhann, G.M., Yan, Y., Wang, C., Zhang, H., Molkentin, J.D., *et al.* (2008). Cyclophilin D deficiency attenuates mitochondrial and neuronal perturbation and ameliorates learning and memory in Alzheimer's disease. Nature medicine *14*, 1097-1105.

Du, H., Guo, L., Yan, S., Sosunov, A.A., McKhann, G.M., and Yan, S.S. (2010). Early deficits in synaptic mitochondria in an Alzheimer's disease mouse model. Proceedings of the National Academy of Sciences of the United States of America *107*, 18670-18675.

Fang, D., Qing, Y., Yan, S., Chen, D., and Yan, S.S. (2016a). Development and Dynamic Regulation of Mitochondrial Network in Human Midbrain Dopaminergic Neurons Differentiated from iPSCs. Stem cell reports *7*, 678-692.

Fang, D., Wang, Y., Zhang, Z., Du, H., Yan, S., Sun, Q., Zhong, C., Wu, L., Vangavaragu, J.R., Yan, S., *et al.* (2015). Increased neuronal PreP activity reduces Abeta accumulation, attenuates neuroinflammation and improves mitochondrial and synaptic function in Alzheimer disease's mouse model. Human molecular genetics *24*, 5198-5210.

Fang, D., Yan, S., Yu, Q., Chen, D., and Yan, S.S. (2016b). Mfn2 is Required for Mitochondrial Development and Synapse Formation in Human Induced Pluripotent Stem Cells/hiPSC Derived Cortical Neurons. Scientific reports *6*, 31462.

Fang, D., Zhang, Z., Li, H., Yu, Q., Douglas, J.T., Bratasz, A., Kuppusamy, P., and Yan, S.S. (2016c). Increased Electron Paramagnetic Resonance Signal Correlates with Mitochondrial Dysfunction and Oxidative Stress in an Alzheimer's disease Mouse Brain. Journal of Alzheimer's disease : JAD *51*, 571-580.

Gan, X., Huang, S., Wu, L., Wang, Y., Hu, G., Li, G., Zhang, H., Yu, H., Swerdlow, R.H., Chen, J.X., *et al.* (2014a). Inhibition of ERK-DLP1 signaling and mitochondrial division alleviates mitochondrial dysfunction in Alzheimer's disease cybrid cell. Biochimica et biophysica acta *1842*, 220-231.

Gan, X., Wu, L., Huang, S., Zhong, C., Shi, H., Li, G., Yu, H., Howard Swerdlow, R., Xi Chen, J., and Yan, S.S. (2014b). Oxidative stress-mediated activation of extracellular signal-regulated kinase contributes to mild cognitive impairment-related mitochondrial dysfunction. Free radical biology & medicine *75*, 230-240.

Guo, L., Du, H., Yan, S., Wu, X., McKhann, G.M., Chen, J.X., and Yan, S.S. (2013). Cyclophilin D deficiency rescues axonal mitochondrial transport in Alzheimer's neurons. PloS one *8*, e54914.

Hartfield, E.M., Yamasaki-Mann, M., Ribeiro Fernandes, H.J., Vowles, J., James, W.S., Cowley, S.A., and Wade-Martins, R. (2014). Physiological characterisation of human iPS-derived dopaminergic neurons. PLoS One *9*, e87388.

Iuso, A., Scacco, S., Piccoli, C., Bellomo, F., Petruzzella, V., Trentadue, R., Minuto, M., Ripoli, M., Capitanio, N., Zeviani, M., *et al.* (2006). Dysfunctions of cellular oxidative metabolism in patients with mutations in the NDUFS1 and NDUFS4 genes of complex I. The Journal of biological chemistry *281*, 10374-10380.

Krencik, R., Weick, J.P., Liu, Y., Zhang, Z.J., and Zhang, S.C. (2011). Specification of transplantable astroglial subtypes from human pluripotent stem cells. Nature biotechnology *29*, 528-534.

Polster, B.M., Nicholls, D.G., Ge, S.X., and Roelofs, B.A. (2014). Use of potentiometric fluorophores in the measurement of mitochondrial reactive oxygen species. Methods in enzymology *547*, 225-250.

Trimmer, P.A., and Borland, M.K. (2005). Differentiated Alzheimer's disease transmitochondrial cybrid cell lines exhibit reduced organelle movement. Antioxidants & redox signaling *7*, 1101-1109.

Williams, E.C., Zhong, X., Mohamed, A., Li, R., Liu, Y., Dong, Q., Ananiev, G.E., Mok, J.C., Lin, B.R., Lu, J., *et al.* (2014). Mutant astrocytes differentiated from Rett syndrome patients-specific iPSCs have adverse effects on wild-type neurons. Human molecular genetics *23*, 2968-2980.

Xu, S., and Chisholm, A.D. (2014). C. elegans epidermal wounding induces a mitochondrial ROS burst that promotes wound repair. Developmental cell *31*, 48-60.